Novel Control Method for the MMC Connected to Wind Farms

Xiangyu Pei, Caoyang Jia, Feng Ji, Hui Pang, *Member*, *IEEE*, *CSEE*, and Guangfu Tang, *Member*, *IEEE*, *Fellow*, *CSEE*

***Abstract*—Large-scale renewable energy transmission via the voltage source converter (VSC) based high-voltage direct current (HVDC) is a crucial development direction for constructing a new-typed power system in China. However, renewable energy is characterized by volatility, intermittency, and randomness. When the sending-end modular multilevel converter (MMC) cannot adapt to the rapid fluctuations in renewable energy output, its energy balance will be disrupted by the active power difference between the AC and DC sides, causing issues such as wideband oscillations and exacerbated circulating currents. To solve the problem mentioned above, a novel energy balance-based control method for MMCs connected to wind farms is proposed in this paper, enabling the MMC to effectively adapt to fluctuations in renewable energy output and naturally maintain circulating current at a relatively low level. Firstly, the evolution principle illustrating topology decomposition and reconfiguration of the MMC is revealed. Secondly, the control method for AC internal voltage is proposed, which combines the energy balance between the half MMCs and voltage amplitude support. Thirdly, the DC internal voltage is defined, and its control method is proposed based on the MMC's overall energy balance. Then, independent control of each bridge arm is achieved by integrating the energy balance of the bridge arms with both the AC and DC internal voltages. Finally, an electromagnetic transient simulation model is built with PSCAD/EMTDC, and the efficacy and practicality of the proposed method are demonstrated through extensive simulation experiments.**

***Index Terms*—DC current control, energy balance control, renewable energy, VSC-based HVDC system.**

I. Introduction

In the present global energy transformation, such renewable energy sources as wind and solar power are regarded as strategic industries capable of addressing both the financial and climate crises, which are critical in promoting global energy transition and sustainable economic and social development [1]. VSC-based HVDC transmission technology provides an efficient solution for seamlessly integrating, reliably transmitting, optimally configuring, and flexibly utilizing large-scale renewable energy [2]–[4]. Therefore, in constructing a new-typed power system with enhanced capacity for renewable energy consumption, the renewable energy delivered by VSC-based HVDC is one of the important methods.

However, renewable energy has significant characteristics such as randomness, intermittency, and volatility [5]. When the output of the renewable energy power station changes rapidly, the inability of the converter station to transmit energy promptly results in energy accumulation, thereby disrupting the overall energy balance. Moreover, the DC outlet voltage of the converter station also rises due to the accumulation of surplus energy, resulting in a DC voltage difference in the DC path between stations. The sudden change of DC voltage between stations causes the uncontrolled DC current to fluctuate, and the DC current causes the energy of submodules to fluctuate through the DC path. As a result, the energy balance of the bridge arms is disrupted, which may induce problems such as wideband oscillations that compromise the system's stable operation [6]. What's worse, the circulating currents resulting from energy imbalance will be exacerbated with the integration of renewable energy, leading to increased system power losses and higher operational expenses [7], [8].

At present, grid-following control is adopted by the majority of renewable energy stations. Thus, VSC-based HVDC transmission technology must apply the voltage and frequency (V/f) control to the sending-end converter station [9]. References [10] and [11] propose a V/f control method based on direct current control, which applies both a voltage outer loop and a current inner loop and provides AC voltage for renewable energy stations. To improve the transmission capacity and reliability, reference [12] proposes a double V/f droop control strategy for bipolar converter stations, which ensures reliable AC voltage output in a bipolar system. Circulating current suppression must be incorporated into the MMC control to maintain stable operation. References [13] and [14] propose circulating current suppressors based on the proportional-integral (PI) controller, which decomposes the detected three-phase circulating current into a direct current component in the dq coordinate system for suppression. Reference [15]–[17] establish mathematical models of the MMC under different operating conditions, calculate the circulating current's ampli-

Manuscript received June 1, 2024; revised July 21, 2024; accepted September 14, 2024. Date of online publication January 10, 2025; date of current version March 3, 2025. This work is supported by the National Natural Science Foundation of China (No. 52277075), and Postgraduate Scientific Research Innovation Project of Changsha University of Science & Technology (No. CSLGCX23062).

X. Y. Pei (corresponding author, email: 646888200@qq.com) is with the State Key Laboratory of Disaster Prevention & Reduction for Power Gird, Changsha University of Science & Technology, Changsha 410114, China, and also with Beijing Huairou Laboratory, Beijing 101400, China.

C. Y. Jia is with the State Key Laboratory of Disaster Prevention & Reduction for Power Gird, Changsha University of Science & Technology, Changsha 410114, China.

F. Ji is with the State Key Laboratory of Advanced Power Transmission Technology, China Electric Power Research Institute Co., Ltd., Beijing 100192, China.

H. Pang and G. F. Tang are with Beijing Huairou Laboratory, Beijing 100084, China.

DOI: 10.17775/CSEEJPES.2024.03920

tude and phase, and propose a circulating current suppression method by injecting a double-frequency current component into the MMC bridge arms. In summary, the existing V/f control methods are designed based on direct current control, which utilizes the regulation of differential-mode and common-mode voltages across bridge arms to facilitate power transmission. Given the difficulty of independently controlling the energy of each bridge arm, additional control methods, such as intricate circulating current control, must be passively introduced to address the problems caused by energy imbalance.

Based on existing MMC's control methods, the bridge arms of each phase unit operate in a coupled control state. In terms of modulation, a few methods integrate the dynamic voltage of the DC reactor with the DC line voltage to provide real-time feedback modulation. Thus, the energy transmitted through the MMC cannot be precisely controlled in real-time, nor can the overall and internal energy balance of the MMC be maintained. Therefore, this paper proposes a novel energy balance-based control method for MMCs connected to wind farms. MMC's energy balance is achieved, enabling MMC to effectively adapt to the fluctuation of renewable energy output and allowing the circulating current to be naturally maintained at a lower level.

The remaining sectors of this paper are organized as follows. The control methods for the typical topology of wind power transmission through a VSC-based HVDC system are introduced in Section II. A new perspective on MMC topology decomposition and reconstruction is proposed in Section III. A novel control method for MMCs in light of the whole energy balance of each bridge arm is proposed in Section IV. Extensive simulation verifications are conducted in Section V. Eventually, some worthwhile conclusions are put forward in Section VI.

II. Basic Principles

A. Topology

The topology of wind power transmission through a VSC-based HVDC system is shown in Fig. 1. PCC is the point

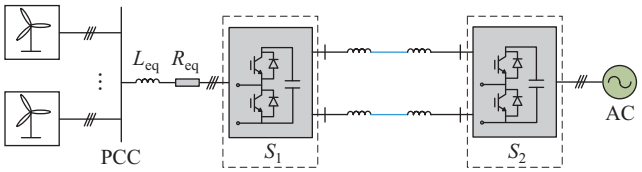

Fig. 1. Topology of wind power transmission through a VSC-based HVDC system.

of common coupling between the wind farms and converter station S_1. L_{eq} and R_{eq} denote the AC line's equivalent inductance and resistance, respectively. S_1 and S_2 are MMC-based converter stations. AC stands for the receiving-end power system.

In Fig. 1, large-scale wind power, featuring "fluctuation, intermittence and randomness", is transmitted to PCC. The power is collected at converter station S_1, where it is converted from AC to DC before being sent over the DC line of the VSC-based HVDC system. Finally, at converter station S_2, the power is reconverted from DC to AC to supply the receiving-end power system for consumption.

B. Control Strategy of Wind Turbines

Generally, the wind farms shown in Fig. 1, consisting of permanent magnet synchronous generator (PMSG)-based wind turbines, adopt grid-following control strategies. The control diagram of PMSG-based wind turbines is presented in Fig. 2.

The machine-side converter (MSC) regulates the generator's speed and the current's d-axis component to achieve maximum power tracking. To minimize the loss of the generator, the d-axis component of the current reference is set to 0. DC voltage and reactive power are managed by the grid-side converter (GSC). Since the wind farms utilize the grid-following control method, a phase-locked loop is needed for the grid-side converter to track the phase of the AC voltage provided by station S_1. Therefore, the wind farms can be regarded as an AC current source.

C. Traditional Control Method

Due to a lack of black-start capability of wind farms shown

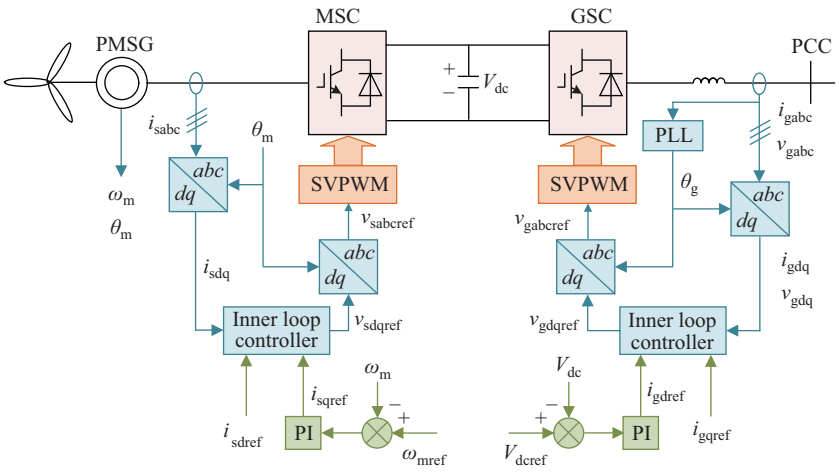

Fig. 2. The control diagram of PMSG-based wind turbine.

in Fig. 1, a stable synchronous AC voltage source needs to be provided by S_1 through V/f control. The control diagram of MMC connected with wind farms is displayed in Fig. 3. S_1 separately controls the d-axis and q-axis components of the AC voltage to equal the voltage amplitude and 0 to provide a stable AC voltage on the valve side of the transformer. Since the V/f control was adopted, S_1 can be regarded as an AC voltage source on the AC side.

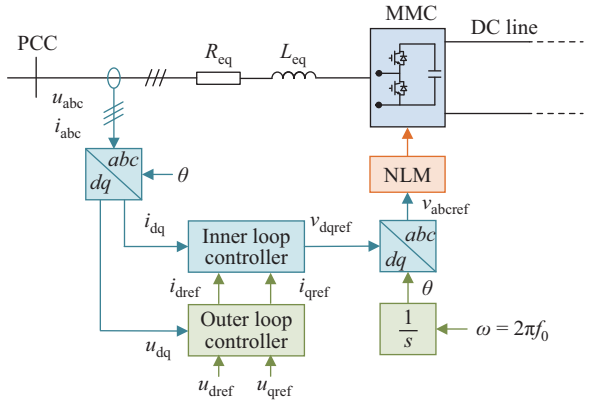

Fig. 3. The traditional control diagram of converter station S_1.

Moreover, the controller gives the phase of AC voltage provided by S_1. After the phase is tracked by GSC, the wind farm will automatically adjust the phase of its AC voltage to guarantee the reliability of power transmission. After receiving the power transmitted by the wind farm, the converter station S_1 will transmit the same amount of power to converter station S_2 to maintain the whole energy balance of converter station S_1.

III. New Perspective Of MMC Topology Analysis

A. Topology Decomposition and Reconstruction

A complete MMC can be depicted in Fig. 4(a) as three-phase units, and each unit contains two bridge arms with symmetrical structures and identical parameters. Each bridge arm contains N cascaded submodules and a reactor in series. The MMC structure is highly modular and can accommodate varying power and voltage levels.

The reconstruction of the MMC topology is shown in Fig. 4(b). Firstly, a bridge arm is configured with N sub-modules and a reactor, all connected sequentially. Secondly, considering the DC reactor, H-MMC comprises three parallel bridge arms in series with a DC reactor. Finally, two H-MMCs with the same design and parameters are connected to form a complete MMC. The DC reactor and H-MMC are involved in the control of MMC together.

B. Operation Principle

The proposed structure of H-MMC is presented in Fig. 5, where u_{sabc} is the AC voltage source, U_{dc} is the voltage on the DC side, T is the converter transformer, e_j (j = a, b, c) represents the voltage across each arm of the bridge, and i_j denotes the current of each bridge arm, v_j and V_{dc} indicate AC and DC internal voltages of the H-MMC, respectively.

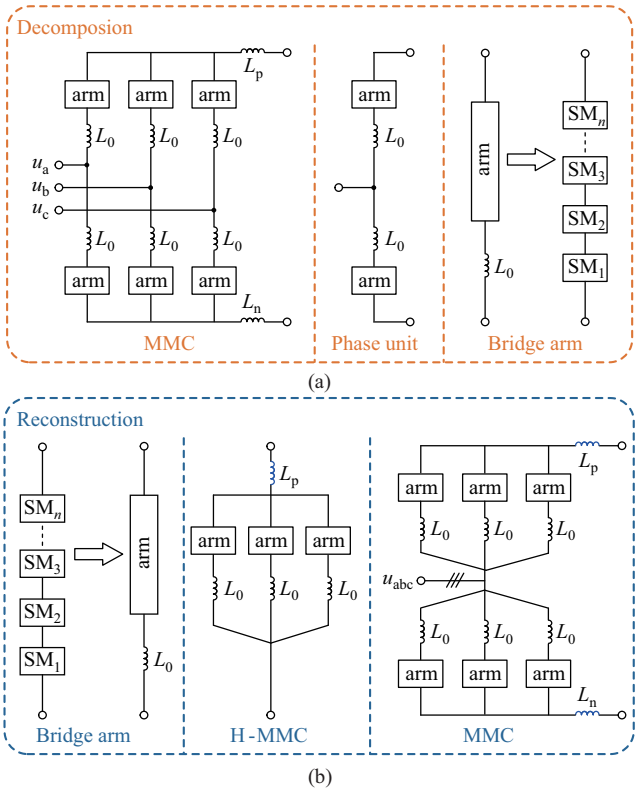

Fig. 4. Topology decomposition and reconstruction of modular multilevel converter. (a) Decomposition. (b) Reconstruction.

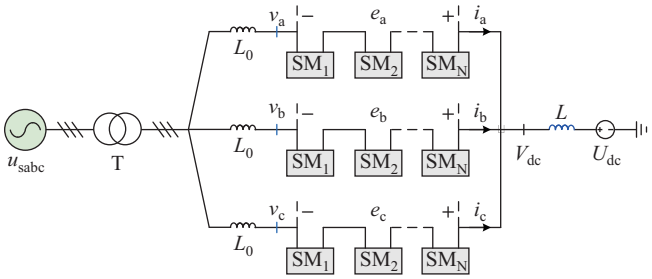

Fig. 5. Proposed structure of H-MMC.

Based on the proposed structure shown in Fig. 5, the power transmitted between u_{sabc} and H-MMC can be derived as:

$$\begin{cases} P = \dfrac{U_{\mathrm{sabc}} V_{\mathrm{abc}}}{X} \sin(\delta_1 - \delta_2) \\ Q = \dfrac{U_{\mathrm{sabc}}(U_{\mathrm{sabc}} - V_{\mathrm{abc}} \cos(\delta_1 - \delta_2))}{X} \end{cases} \tag{1}$$

where U_{sabc} is the RMS value of the AC voltage source u_{sabc}, V_{abc} is the RMS value of the H-MMC's internal voltage, X denotes the equivalent impedance between AC voltage source and H-MMC, δ_1 and δ_2 are the phase angle of U_{sabc} and V_{abc}, respectively. Therefore, the power transmission between the AC system and the H-MMC can be controlled by adjusting the H-MMC's AC internal voltage.

The power transmitted between i_{abc} and H-MMC can also be derived as:

$$\begin{cases} p = \boldsymbol{v} \cdot \boldsymbol{i} = \mathrm{dot}(\boldsymbol{v}, \boldsymbol{i}) \\ q = \boldsymbol{v} \times \boldsymbol{i} = \mathrm{cross}(\boldsymbol{v}, \boldsymbol{i}) \end{cases} \tag{2}$$

where v and i are the voltage vector and current vector respectively. Thus, when the H-MMC is connected to a system that can be equivalent to an AC current source, such as wind farms, the power transmission is achieved by regulating the AC internal voltage of the H-MMC.

The simplified equivalent structure of H-MMC connected to wind farms can be shown in Fig. 6. Each bridge arm's output voltage reference of each bridge arm can be expressed by

$$e_{j\mathrm{ref}} = V_{\mathrm{dc}} - v_j \tag{3}$$

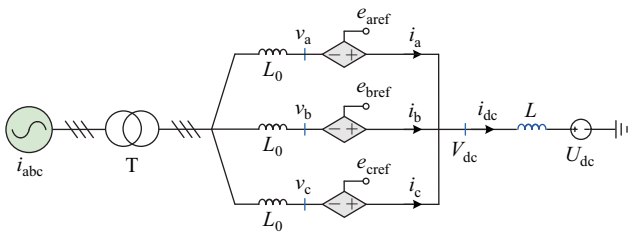

Fig. 6. Simplified equivalent structure of the H-MMC.

Therefore, by modulating the MMC and balancing the submodule capacitor voltage, the output voltage e_j is nearly consistent with the output voltage reference $e_{j\mathrm{ref}}$.

C. Verification

To validate the feasibility of the proposed H-MMC, an electromagnetic transient model of H-MMC connected to power systems is built with PSCAD/EMTDC, adhering to the configuration depicted in Fig. 5. The simulation model's main parameters are displayed in Table I. The power transmitted from u_{sabc} to H-MMC is controlled by adjusting the H-MMC's internal voltage output phase.

TABLE I
PARAMETERS OF H-MMC

Items	Value
Voltage of the AC system (kV)	230
Frequency of the AC system (Hz)	50
DC rated voltage (kV)	250
Transformer ratio	230/290.88
Rated capacity (MVA)	850
SM capacity rated voltage (kV)	2.2
SM capacitance (mF)	8
Arm inductance (mH)	100
Number of SMs per arm	244

An AC voltage source of which the amplitude and frequency are 230 kV and 50 Hz respectively is interfaced with the H-MMC via a transformer. The active power is transmitted to the DC voltage source with an amplitude of 250 kV. In Fig. 7(a) and (b), the current and voltage in the bridge arms of the H-MMC exhibit symmetry and equilibrium. As depicted in Fig. 7(c), the reference value can be precisely tracked by each bridge arm's output voltage.

IV. Proposed Novel Control Method

Taking into account S_1 in Fig. 1 as a controlled source, the topology of MMC connected to the wind farm in the form of a controlled source is presented in Fig. 8, where i_{abc} is the

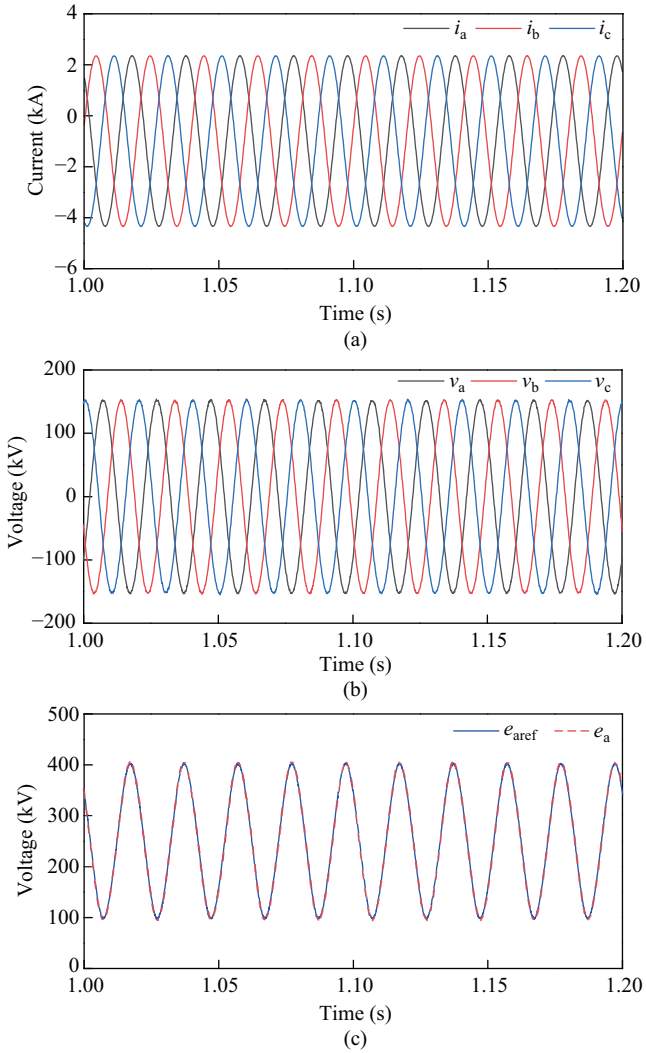

Fig. 7. Simulation Result of H-MMC. (a) Arm current. (b) AC internal voltage. (c) Arm voltage of phase A.

equivalent current source of the wind farm, u_k (k = p, n) is the DC external voltage of MMC. Considering the analysis in Section II, station S_1 needs to adopt a "grid-forming" control with constant voltage amplitude and frequency to ensure power transmission. Besides, in the existing system research shown in Fig. 1, the DC line voltage is generally controlled by S_2. Thus, an appropriate and feasible control method, based on the equivalent current source i_{abc} and DC external voltage u_k of MMC, is crucial to ensuring the converter station's continuous, steady operation.

A. AC Voltage Control

Disassembling the converter station shown in Fig. 8 into a combination of upper H-MMC and lower H-MMC, the AC internal voltage reference of H-MMCs is displayed as:

$$\begin{cases} v_{\mathrm{apref}} = v_{\mathrm{anref}} = U_{\mathrm{m}} \cos(2\pi f t + \theta) \\ v_{\mathrm{bpref}} = v_{\mathrm{bnref}} = U_{\mathrm{m}} \cos\left(2\pi f t - \dfrac{2\pi}{3} + \theta\right) \\ v_{\mathrm{cpref}} = v_{\mathrm{cnref}} = U_{\mathrm{m}} \cos\left(2\pi f t + \dfrac{2\pi}{3} + \theta\right) \end{cases} \tag{4}$$

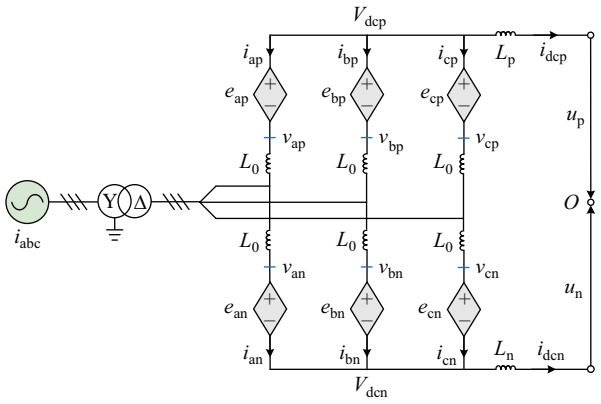

Fig. 8. Topology of MMC connected to wind farms in form of controlled source.

where θ, U_{m} and f represent each internal voltage's phase angle, amplitude and frequency, respectively.

Moreover, in Fig. 9, by representing the H-MMC as a controlled voltage source, the power transmission between two H-MMCs is managed by adjusting the H-MMC's phase angle. By defining the sum of submodules' energy in each bridge arm as bridge arm energy E_{jk}, the overall energy of MMC can be expressed by the sum of all bridge arm energy. The bridge arm energy can be calculated as:

$$E_{jk} = \sum_{i=1}^{N} \frac{1}{2} C_{\mathrm{sm}i} U_{\mathrm{sm}i}^2 \tag{5}$$

where N represents the number of submodules in series in each bridge arm.

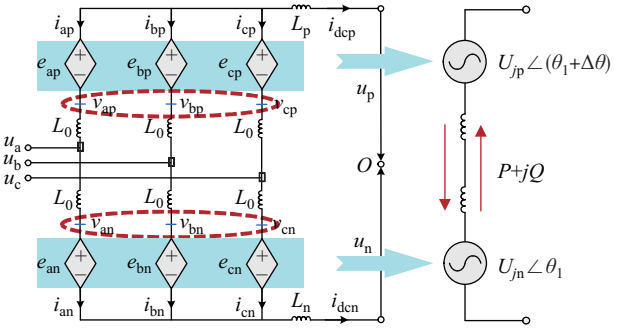

Fig. 9. Power transmission between two H-MMC.

Therefore, a control method for H-MMC energy balancing is proposed to achieve the energy balance of two H-MMCs. The phase angle $\Delta\theta$ would be adjusted by comparing the energy difference between H-MMCs, as shown in Fig. 10, where $E_{\text{H-MMCp}}$ and $E_{\text{H-MMCn}}$ represent the overall energy of upper H-MMC and lower H-MMC. When $E_{\text{H-MMCp}}$ is greater than $E_{\text{H-MMCn}}$, $\Delta\theta$ will be a positive value so that the energy will flow from H-MMC$_{\mathrm{p}}$ to H-MMC$_{\mathrm{n}}$.

Besides, to preserve the voltage on either side of the transformer at the specified value, a voltage amplitude support controller for the transformer's valve side is proposed based on the negative feedback control theory. In Fig. 11, V_{MMCref} represents the voltage amplitude reference on the valve side

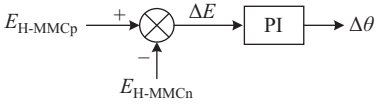

Fig. 10. Structure of H-MMC energy balance controller.

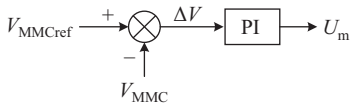

Fig. 11. Voltage amplitude support controller for the transformer's valve side.

of the transformer, whereas V_{MMC} is the actual voltage amplitude. With the PI controller, the voltage reference V_{MMCref} can be tracked precisely.

The equivalent diagram of the MMC's AC side connected to wind farms is shown in Fig. 12, and v_{abc} is the AC output internal voltage of each phase.

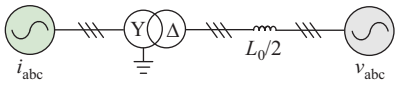

Fig. 12. Equivalent diagram of the MMC's AC side connected to wind farms.

According to (2), when the current source i_{abc} operates at its rated state, the power transmission between i_{abc} and the MMC can be achieved by controlling the AC internal voltage of the MMC. Furthermore, in the wind power transmission through a VSC-based HVDC system depicted in Fig. 1, the AC internal voltage of S_1 maintains a steady amplitude and frequency, which causes the variations in the current's amplitude in response to the power sent by the wind farm.

B. DC Current Control

Based on the principle of energy balancing, the structure of DC current controller can be shown in Fig. 13, where E_{total} and E_{MMCset} are the real value and rated value of the whole energy of MMC, respectively. i_f denotes the DC current's real-time tracking value, which is obtained by dividing the active power by the DC voltage. i_{dcref} is the DC current reference of MMC. In addition, E_{MMCset} and i_f can be calculated as

$$\begin{cases} E_{\text{MMCset}} = 6NE_{\mathrm{sm}} \\ i_{\mathrm{f}} = P_{\mathrm{ac}}/E_{\mathrm{dc}} \end{cases} \tag{6}$$

where E_{sm} is the rated energy of the submodule, E_{dc} is the DC voltage of the MMC, and P_{ac} is the active power flowing into the MMC.

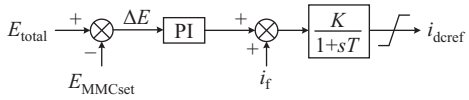

Fig. 13. Structure of DC current controller.

In Fig. 13, the DC current reference i_{dcref} is related to the whole energy of MMC and the energy flowing into MMC's AC side. Thus, the proposed DC current controller could stabilize

the MMC's energy fluctuation. Moreover, to ensure the DC current operates within a safe range, a limiter is added to limit the amplitude of i_{dcref}.

C. Bridge Arm Voltage Reference Control

1) DC Internal Voltage Calculation

With reference to Fig. 8, the DC internal voltage $V_{\mathrm{dc}k}$ can be described as:

$$\begin{cases} V_{\mathrm{dcp}} = u_{\mathrm{Lp}} + u_{\mathrm{p}} \\ V_{\mathrm{dcn}} = u_{\mathrm{Ln}} + u_{\mathrm{n}} \end{cases} \tag{7}$$

where u_{Lp} and u_{Ln} are the voltage across the DC reactors.

The voltage across the reactor can be written as:

$$u_{\mathrm{L}} = L\frac{\Delta i}{\Delta T} \tag{8}$$

where ΔT is the sampling period, Δi is the variation of current in the sampling period. Thus, (5) can be transformed to

$$\begin{cases} V_{\mathrm{dcp}} = L_{\mathrm{p}}\dfrac{\Delta i_{\mathrm{dcp}}}{\Delta T} + u_{\mathrm{p}} \\ V_{\mathrm{dcn}} = L_{\mathrm{n}}\dfrac{\Delta i_{\mathrm{dcn}}}{\Delta T} + u_{\mathrm{n}} \end{cases} \tag{9}$$

where Δi_{dcp} and Δi_{dcn} are the variation of current flowing via the DC reactors during the sampling period. The structure of DC internal voltage calculation controller is introduced in Fig. 14, where i_{dcref} is the current reference generated by DC current controller shown in Fig. 13.

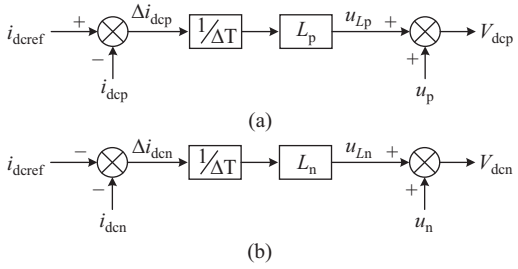

Fig. 14. Structure of DC internal voltage calculation controller. (a) Positive pole. (b) Negative pole.

2) Voltage Reference Adjustment

To guarantee the whole energy balance of each bridge arm, monitoring all arm energy of MMC and involving the surplus or loss of energy in voltage reference control of each bridge arm is crucial. The control structure of the voltage reference adjustment controller for each bridge arm can be shown in Fig. 15. E_{jk} and E_{set} are the real value and rated value of the total energy of the bridge arm, respectively. Δv_{jk} serves as the voltage reference correction of bridge arms.

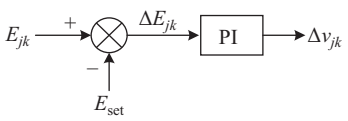

Fig. 15. Structure of voltage reference adjustment controller.

3) Voltage Reference of Bridge Arms Generation

As seen in Fig. 16, the voltage reference of bridge arms for the upper H-MMC can be generated by subtracting internal voltage reference $v_{j\mathrm{pref}}$ from DC voltage V_{dcp} of H-MMC and adding the correction value $\Delta v_{j\mathrm{p}}$. For the lower H-MMC, the voltage reference of bridge arms can be produced by subtracting DC voltage V_{dcn} of H-MMC from internal voltage reference $v_{j\mathrm{nref}}$ and adding the correction value $\Delta v_{j\mathrm{n}}$. Moreover, the voltage reference $e_{jk\mathrm{ref}}$ should be limited for safety and stability of operation. Based on the operating characteristic of MMC, the upper and lower bounds of $e_{jk\mathrm{ref}}$ should be set to NV_{c} and 0 respectively.

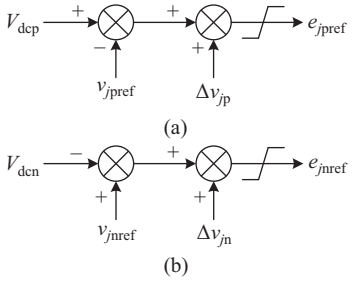

Fig. 16. Voltage reference of bridge arms generation. (a) Upper H-MMC. (b) Lower H-MMC.

It is worth mentioning that the bridge arm will selectively input the submodules in accordance with the voltage reference upon receiving the voltage reference command and then output the real voltage of the bridge arms.

D. Overall Control Structure

The entire control structure of station S_1 can be shown in Fig. 17. The control objectives for S_1 are DC current and AC voltage. Firstly, the DC current reference i_{dcref} and AC internal voltage reference $v_{jk\mathrm{ref}}$ are generated by outer loop controller. Secondly, the inner loop controller obtains the DC internal voltage $V_{\mathrm{dc}k}$ with DC current reference i_{dcref}, DC

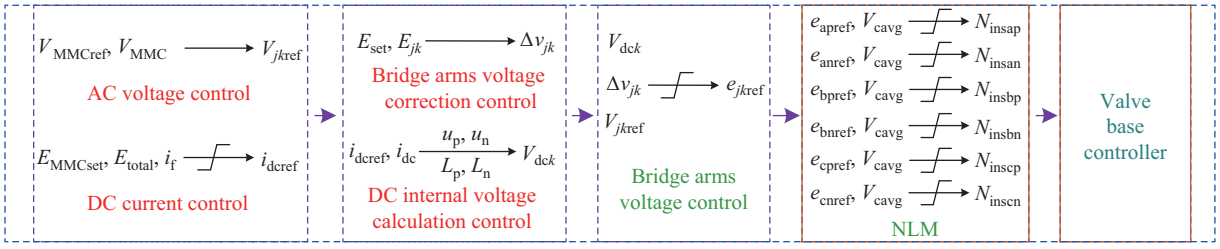

Fig. 17. Overall control structure.

outlet current $i_{\mathrm{dc}k}$ and DC external voltage u_k. Then, the voltage reference correction Δv_{jk} is generated based on voltage reference adjustment. Finally, the voltage reference of each bridge arm is calculated with the DC internal voltage $V_{\mathrm{dc}k}$, AC internal voltage $v_{jk\mathrm{ref}}$ and voltage reference correction Δv_{jk}.

Station S_1 performs nearest-level modulation to determine the number N_{ins} of submodules to be inserted in each bridge arm based on the voltage reference $e_{jk\mathrm{ref}}$ and the corresponding voltages of all cascaded submodule capacitors. The valve base controller then determines the control instructions for each bridge arm according to N_{ins}. Finally, the working state of each bridge arm submodule is controlled by MMC with the control instructions.

V. Simulation Verifications

To verify the effectiveness and feasibility of the proposed control method, a wind power transmission through a $\pm$ 500 kV two-terminal VSC-based HVDC system electromagnetic transient model, as shown in Fig. 18, is built with PSCAD/EMTDC. Each wind farm adopts the wind turbines depicted in Fig. 2, and the full power converter parameters are given in Table II. Each wind farm transmits 800 MW of active power to converter station S_1 respectively. The VSC-based HVDC system operates in bipolar mode with a metallic return grounded through a resistance of 15 Ω in converter station S_2. S_1 and S_2 are modular multilevel converters with half-bridge submodules, and the main parameters are illustrated in Table III. S_1 adopts the proposed novel control method and S_2 adopts the conventional V_{dc}/Q control method. Without loss of generality, the analysis in this section centers on the positive pole of the VSC-based HVDC system.

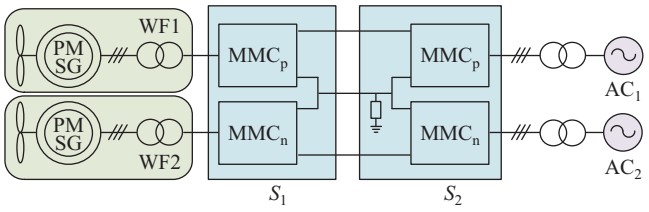

Fig. 18. Wind power transmission through a $\pm$ 500 kV two-terminal VSC-based HVDC system.

TABLE II
Parameters of the Full Power Converter

Converter	Machine side	Grid side
Converter	Two-level PWM	Two-level PWM
RMS value of AC side line voltage (kV)	0.69	0.69
Voltage ratio of transformer	–	0.69 kV/35 kV
Leakage reactance of transformer (p.u.)	–	0.08
Rated capacity of transformer (MVA)	–	5.8
DC side rated voltage (kV)	1.45	
DC side capacitance (mF)	50	

A. Normal Operation

In Fig. 19(a), the active power is transmitted from the wind farm at 3 s, and reaches its rated power of 800 MW at approximately 3.4 s. At 4 s, the active power transmitted from the wind farm starts to decrease and eventually drops to 0 at around 4.4 s. Then, the active power increases again, reaching 800 MW at about 5.4 s. As shown in Fig. 19(b), it can be observed that the RMS value of the line voltage on the transformer's valve side is maintained at the specified 275 kV with the voltage amplitude support controller. As shown in Fig. 19(c), the change of the valve side current is identical to that of the active power due to the constant valve side line voltage. Similarly, the variation trend of the DC current reference i_{dcref}, shown in Fig. 19(d), also parallels the active power with the proposed DC current control method, and the DC outlet current i_{dc} can achieve accurate real-time tracking of i_{dcref} with the proposed novel control method. In addition, Fig. 19(e) and (f) demonstrate that the energy of MMC only fluctuates slightly as the active power varies, and the energy of upper and lower H-MMCs remains balanced owing to the energy balancing control.

TABLE III
System Parameters of the VSC-based HVDC System

Items	S_1	S_2
Topology	Bipolar	Bipolar
AC system voltage (kV)	220	525
DC rated voltage (kV)	500	500
Control mode	$I_{\mathrm{dc}} + V_{\mathrm{ac}}$	$V_{\mathrm{dc}} + Q_{\mathrm{ac}}$
Transformer ratio	220/275	290.88/525
Rated capacity (MVA)	850	850
SM capacity rated voltage (kV)	2.2	2.2
SM capacitance (mF)	15	15
Arm inductance (mH)	100	100
Number of SMs per arm	244	244

B. Circulating Current Analysis

This section conducts a comprehensive analysis of the circulating current to further improve the proposed novel control method.

Without loss of generality, the current of Phase A upper bridge arm is employed for circulation analysis. As depicted in Fig. 20, the bridge arm's current consists of DC and AC components. The arm current's fast Fourier transform (FFT) results are shown in Fig. 21. The dominant frequency component is identified at 50 Hz, with a magnitude of 1.229 kA, aligning with the system's fundamental frequency. The magnitude of the second harmonic component is 0.022 kA, whereas the DC component is recorded with 0.52 kA.

As summarized in Table IV, the second harmonic ratio, defined as the ratio of the RMS value of the second harmonic component to the DC component, is compared with two distinct circulating current suppression methods described in Reference [18] and [19]—the conventional circulating current suppressing controllers (CCSC) and the internal model control

TABLE IV
FFT Harmonic Analysis Parameters Under Different MMC Circulation Models

Control Method	CCSC [18]	IMC [19]	Proposed method
Second harmonic ratio	2.80%	3.07%	3.00%

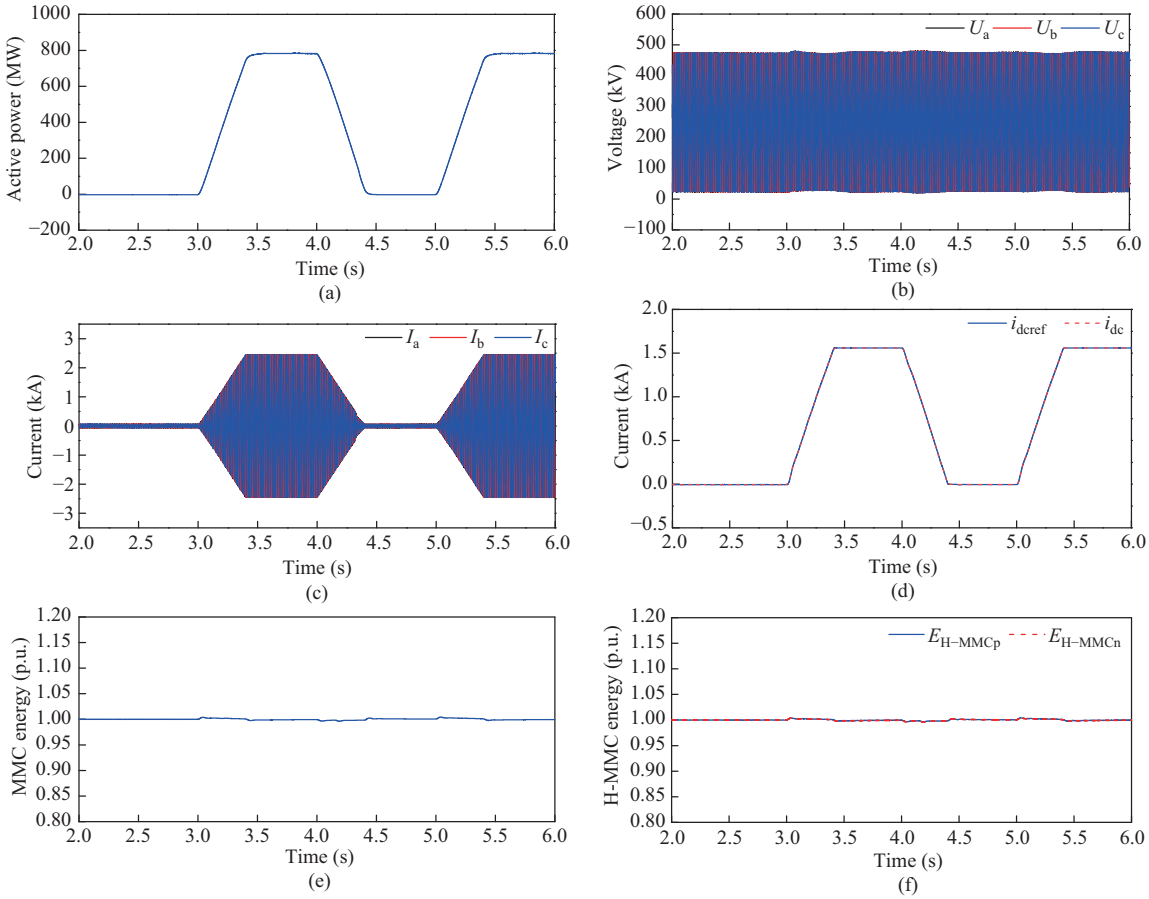

Fig. 19. Simulation Results. (a) Active power. (b) Voltage on transformer's valve side. (c) Current on transformer's valve side. (d) DC current reference and DC outlet current. (e) Energy of MMC. (f) Energy of H-MMCs.

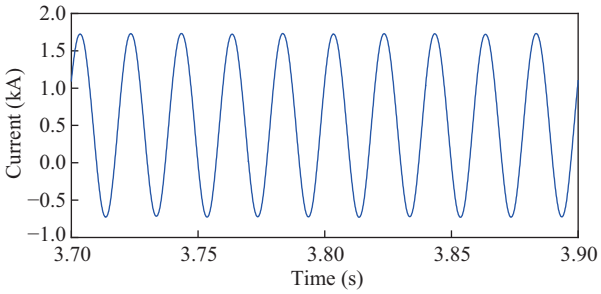

Fig. 20. Phase A upper bridge arm current.

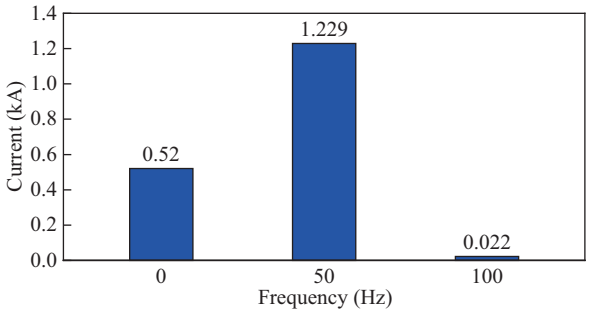

Fig. 21. Fast Fourier transform results of arm current.

(IMC). With the energy balance of bridge arms, the proposed method maintains a relatively low circulating current level, achieving a second harmonic ratio of 3.00%, nearly identical to those of the conventional CCSC method (2.80%) and the IMC control (3.07%). Notably, no other circulating current suppression methods are included in the proposed method. Therefore, further optimization of the proposed method could reduce circulating currents to even lower levels, providing a more effective solution.

VI. Conclusion

To achieve energy balance in the MMC and facilitate the large-scale integration and consumption of renewable energy, a new perspective on topology decomposition and reconstruction for the MMC is presented first, based on which a novel energy balance-based control method for MMCs connected to wind farms is proposed in this paper. A series of typical simulation results sufficiently validate the effectiveness and practicality of the proposed method. Some valuable conclusions can be drawn as follows.

1) Based on the topology decomposition and reconstruction of the MMC, the H-MMC's basic operation and control principles are proposed. Therefore, a complete MMC can be envisioned as a combination of two H-MMCs with identical structure and parameters.

2) The whole energy balance of the MMC is achieved and

no longer affected by fluctuations in renewable energy output. Additionally, rapid changes in renewable energy output can be effectively tracked by the DC-side active power output, ensuring the smooth integration of renewable energy.

3) The independent control of the bridge arms is achieved with the proposed method. As a result, the circulating current of MMC is naturally maintained at a low level, reducing power losses and system costs.

The proposed method will be further improved to ensure it functions well when applied to MMC under various application requirements.

REFERENCES

[1] H. Zhu, H. Li, G. J. Liu, Y. Ge, J. Shi, H. Li, and N. Zhang, "Energy storage in high variable renewable energy penetration power systems: technologies and applications," *CSEE Journal of Power and Energy Systems*, vol. 9, no. 6, pp. 2099–2108, Nov. 2023.

[2] M. Moradi-Sepahvand and T. Amraee, "Hybrid AC/DC transmission expansion planning considering HVAC to HVDC conversion under renewable penetration," *IEEE Transactions on Power Systems*, vol. 36, no. 1, pp. 579–591, Jan. 2021.

[3] A. Nami, J. L. Rodriguez-Amenedo, S. Arnaltes, M. Á. Cardiel-Álvarez, and R. A. Baraciarte, "Control of the parallel operation of DR-HVDC and VSC-HVDC for offshore wind power transmission," *IEEE Transactions on Power Delivery*, vol. 37, no. 3, pp. 1682–1691, Jun. 2022.

[4] Z. P. Shen, J. B. Zhu, L. J. Ge, S. Q. Bu, J. B. Zhao, C. Y. Chung, X. L. Li, and C. S. Wang, "Variable-inertia emulation control scheme for VSC-HVDC transmission systems," *IEEE Transactions on Power Systems*, vol. 37, no. 1, pp. 629–639, Jan. 2022.

[5] J. Z. Liu, Z. M. Du, Q. H. Wang, H. B. Fan, and C. Liu, "Development paths for next-generation coal-fired power generation under new electric power systems," *New Type Power Systems*, vol. 2, no. 24, pp. 357–370, Nov. 2024.

[6] S. M. Zheng, Y. M. Liu, P. Dong, C. Lin, F. Ji, and X. Y. Pei, "Analysis of sub/super-synchronous oscillation between wind farm and MMC in Zhangbei project," *Journal of Global Energy Interconnection*, vol. 6, no. 6, pp. 608–617, Nov. 2023.

[7] Q. R. Tu, Z. Xu, X. Zheng, and M. Y. Guan, "Mechanism analysis on the circulating current in modular multilevel converter based HVDC," *High Voltage Engineering*, vol. 36, no. 2, pp. 547–552, Feb. 2010.

[8] Q. R. Tu, Z. Xu, M. Y. Guan, X. Zheng, and J. Zhang, "Design of circulating current suppressing controllers for modular multilevel converter," *Automation of Electric Power Systems*, vol. 34, no. 18, pp. 57–61, 83, Sep. 2010.

[9] R. Rosso, X. F. Wang, M. Liserre, X. N. Lu, and S. Engelken, "Grid-forming converters: control approaches, grid-synchronization, and future trends—a review," *IEEE Open Journal of Industry Applications*, vol. 2, pp. 93–109, Apr. 2021.

[10] M. Y. Guan and Z. Xu, "Modeling and control of modular multilevel converter based VSC-HVDC system connected to passive networks," *Transactions of China Electrotechnical Society*, vol. 28, no. 2, pp. 255–263, Feb. 2013.

[11] M. Y. Guan and Z. Xu, "Direct voltage control of MMC-based VSC-HVDC system for passive networks," *Electric Power Automation Equipment*, vol. 32, no. 12, pp. 1–5, Dec. 2012.

[12] N. Mei, B. Yuan, T. Li, D. Xu, and G. W. Li, "Study on control strategy of bipolar VSC station connected to islanded renewable power plant," *Power System Technology*, vol. 42, no. 11, pp. 3575–3582, Nov. 2018.

[13] B. Bahrani, S. Debnath, and M. Saeedifard, "Circulating current suppression of the modular multilevel converter in a double-frequency rotating reference frame," *IEEE Transactions on Power Electronics*, vol. 31, no. 1, pp. 783–792, Jan. 2016.

[14] Q. R. Tu, Z. Xu, and L. Xu, "Reduced switching-frequency modulation and circulating current suppression for modular multilevel converters," *IEEE Transactions on Power Delivery*, vol. 26, no. 3, pp. 2009–2017, Jul. 2011.

[15] J. Wang, X. Han, H. Ma, and Z. H. Bai, "Analysis and injection control of circulating current for modular multilevel converters," *IEEE Transactions on Industrial Electronics*, vol. 66, no. 3, pp. 2280–2290, Mar. 2019.

[16] M. X. Wang, W. J. Jiang, and K. Ma, "Circulating current controls for optimal thermal stress of capacitors in MMC systems," *IEEE Transactions on Power Electronics*, vol. 39, no. 10, pp. 12435–12445, Oct. 2024.

[17] R. Chakraborty and A. Dey, "Circulating current control of modular multilevel converter with reduced conduction loss for medium-voltage applications," *IEEE Transactions on Industrial Electronics*, vol. 68, no. 10, pp. 9014–9023, Oct. 2021.

[18] X. F. Yang, Z. J. Li, and T. Q. Zheng, "A novel MMC circulating current suppressing strategy based on virtual impedance sliding mode control," *Proceedings of the CSEE*, vol. 38, no. 23, pp. 6893–6904, Dec. 2018.

[19] H. Li, P. Zhang, and S. J. Liu, "Transient analysis of MMC circulating current suppression strategy," *Power System Protection and Control*, vol. 49, no. 2, pp. 30–38, Jan. 2021.

Xiangyu Pei received the B.Sc., M.Sc. and Ph.D. degrees in Central South University, Huazhong University of Science and Technology, China Electric Power Research Institute in 2012, 2015 and 2019, respectively. He is currently with School of Electrical & Information Engineering, Changsha University of Science & Technology, Changsha, Hunan province, China. His research interests are new-typed power systems construction technology, medium and high voltage DC breaking technology and HVDC transmission line protection.

Caoyang Jia received the B.Sc. degree in Henan Polytechnic University in 2022. He is currently working toward the M.Sc. degree with School of Electrical & Information Engineering, Changsha University of Science & Technology, Changsha, Hunan province, China. His research focuses on new-typed power systems construction technology.

Feng Ji received the bachelor degree in Electrical Engineering from Xi'an Jiaotong University, Xi'an, China, in 2005. In 2011, he received the master degree in Electrical Engineering from North China Electric Power University, Baoding, China. He is currently a professorate senior engineer at China Electric Power Research Institute (CEPRI). His major research field is modeling and simulation technology of power system.

Hui Pang received the B.Eng. and M.Eng. degrees in Electrical Engineering from Hefei University of Technology, China in 2002 and 2005, respectively, and the Ph.D. degree in Electrical Engineering from China Electric Power Research Institute (CEPRI) in 2010. His research focuses on power electronics technology, high-voltage and large-capacity power electronic equipment, high-precision and rapid simulation technology for the new-typed power system.

Guangfu Tang received the B.Eng. degree in Electrical Engineering from Xi'an Jiao Tong University, Shanxi, PR. China, in 1990, and the M.Eng. degree and the Ph.D. degree in Electrical Engineering from Institute of Plasma Physics, the Chinese Academy of Sciences (ASIPP), Hefei, China, in 1993 and 1996 respectively. During 1996-1998, he had a postdoctoral position with China Electric Power Research Institute (CEPRI), Beijing, P.R. China, and he was the vice director of China Energy Conservation Center, Beijing, China. Since 2002, he has been a professor level senior engineer of CEPRI. In 2012, he joined State Grid Smart Grid Research Institute (SGRI), Beijing, China, as the manager of HVDC department. He is now an Academician with the Chinese Academy of Engineering.